2021

Subsurface Structures along Western Yucatan from Integrated Geophysical Analysis

Irina Filina

Lucas Hartford

Published in *Marine and Petroleum Geology* 127 (2021), 104964; doi: 10.1016/j.marpetgeo.2021.104964

Submitted August 26, 2020; revised January 8, 2021; accepted February 4, 2021; published online February 11, 2021.

Subsurface Structures along Western Yucatan from Integrated Geophysical Analysis

Irina Filina[1] and Lucas Hartford[2]

1. Department of Earth and Atmospheric Sciences, University of Nebraska–Lincoln, Lincoln, Nebraska, USA
2. Terracon Consultants, Omaha, Nebraska, USA

Corresponding authors – Irina Filina, University of Nebraska–Lincoln, 223 Bessey Hall, Lincoln, NE, 68510, USA, email ifilina2@unl.edu; Lucas Hartford, Terracon Consultants, 15080 A Cir, Omaha, NE, 68144, USA, email lucas.hartford@outlook.com

Abstract

Integration of seismic, gravity, and magnetic data revealed variations in crustal architecture along the Yucatan passive continental margin. The crust beneath the Yucatan salt basin is ~10 km thick and is primarily a lower continental crust. In contrast, the crust beneath the Campeche salt basin is thicker and comprises both the upper and the lower crustal layers. These variations in crustal architecture explain the strikingly different tectonic histories of these basins outlined by previous authors. The rifting of the Yucatan margin was associated with extensive magmatism expressed as voluminous igneous intrusions in the lower crust, one of which is manifested as the Campeche magnetic anomaly. The zone of extrusive volcanic flows is also interpreted in the northern Yucatan coincident with the Seaward Dipping Reflectors (SDR) in seismic data. Integrated analysis of potential fields and seismic data demands high density and magnetic susceptibility for the rocks of the SDR zone. The presalt sedimentary basin with up to 5 km of sediments overlies the stretched and intruded continental crust adjacent to the Ocean-Continent boundary (OCB). This pre-salt basin is up to 100 km wide and pinches out at the northeastern tip of the Yucatan peninsula. It appears to be compartmentalized with the width of individual segments up to 100 km. All the tectonic elements, namely OCB, SDR, pre-salt sedimentary basin, and magmatic intrusions within the stretched continental crust, have their counterparts in the northeastern Gulf of Mexico and therefore represent important constraints for the prebreakup locations of individual crustal blocks.

Keywords: Gulf of Mexico, rifting, passive continental margin, crustal structures, seaward dipping reflectors, volcanic-rich margin, integrated geophysical analysis

1. Introduction

The Gulf of Mexico is one of the most prolific petroleum basins in the world. Despite the exploration of the gulf that began more than a century ago, it remains a frontier basin (Whaley, 2006; Dribus, 2008; Galloway, 2009; Davison et al., 2015) with the northern part of the basin (the US sector) much more thoroughly explored than the Mexican sector in the south. Recently, the Mexican government lifted the moratorium on exploration in the Mexican sector (Seelke et al., 2013). This paper focuses on the western margin of the Yucatan peninsula in the Southern Gulf of Mexico (Fig. 1) where two salt basins are present (Hudec et al., 2013)—the Yucatan salt basin in the north and the Campeche in the southwest. Several seismic reflection lines across the western margin of the Yucatan peninsula were recently published (Williams-Rojas et al., 2012; Miranda-Peralta et al., 2014; Saunders et al., 2016; Horn et al., 2017; O'Reilly et al., 2017; Steier and Mann, 2019, Fig. 2). These seismic cross-sections indicate several kilometers of sediment beneath the salt (Fig. 2). The base of this pre-salt sedimentary sequence is not always mapped confidently in seismic data. One of the objectives of this paper is to understand the distribution of pre-salt sediments using the joint analysis of published seismic cross-sections with potential fields (gravity and magnetic data).

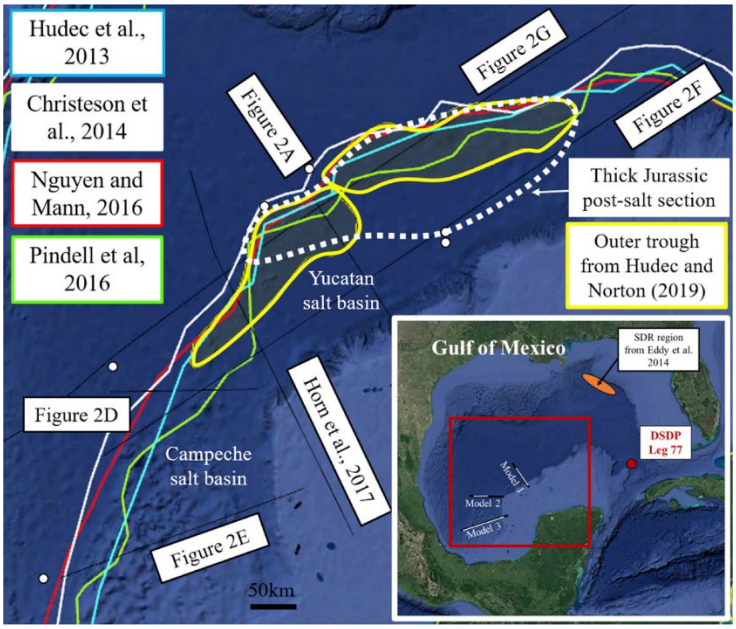

Figure 1. The inset map shows the study area (red box) in the southern Gulf of Mexico. The location of three integrated geophysical models from this study are shown in black with white segments being the extents of seismic cross-sections. The red circle is the DSDP well used to constrain the physical properties of the upper crust. The orange oval in the northeastern Gulf of Mexico represents the region with seaward dipping reflectors (SDR)

from Eddy et al. (2014). Different colors in the main map show the location of Ocean-Continent Boundaries (OCB) from different published models. The black lines are seismic sections used for the study (Fig. 2). White circles show vintage refraction data from Ewing et al. (1960) and Ibrahim et al. (1981) that were used to constrain the depths to Moho. The white dashed outline is the zone of the Jurassic post-salt thickening mapped from seismic data shown in Figure 2, while the yellow polygon is the outer trough mapped by Hudec and Norton (2019).

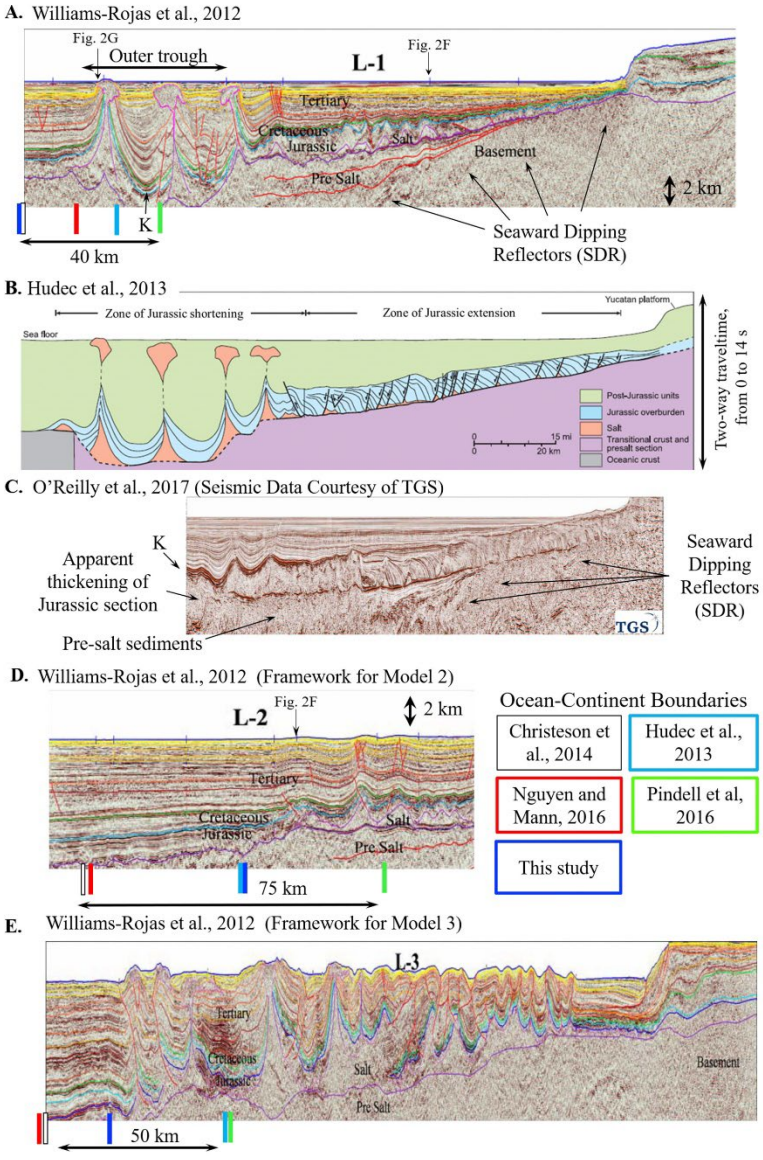

Figure 2. *Continued next page*

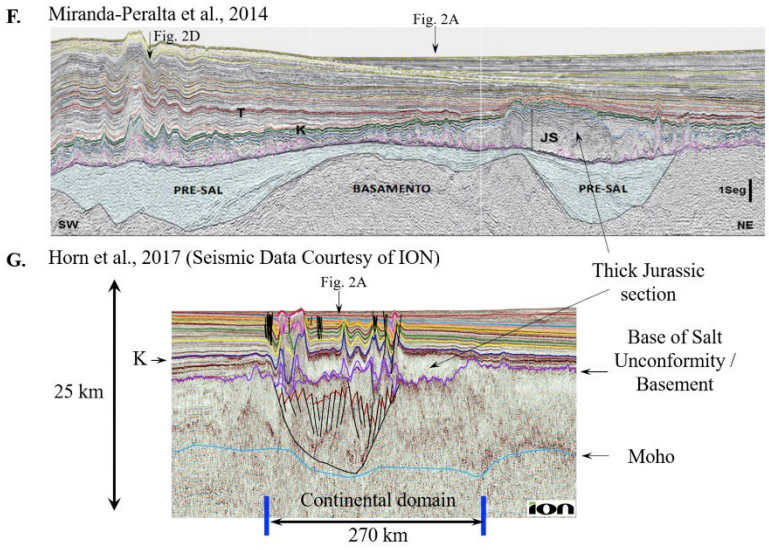

Figure 2. Seismic cross-sections used for the study. Lines shown in sections A, B, and C were utilized for integrated geophysical Model 1. The outer trough associated with an up to 2 km drop in the basement near the OCB is approximately 40 km wide. It is located within the zone of Jurassic shortening identified by Hudec et al. (2013) in section B. Please note the apparent thickening of the Jurassic supra-salt sediments over the outer trough that is clearly seen in section C. The bars of different colors show the location of the OCB from various tectonic models (see Fig. 1). The base of the pre-salt section is partially interpreted in sections A and D, which were used for integrated geophysical Models 1 and 2, respectively; no base of the pre-salt section is interpreted in section E (served as a framework for Model 3). Two strike lines (sections F and G) were also utilized as constraints for modeling. The vertical scale of the seismic line in section F is the two-way travel time in seconds; it shows up to 2 s thick pre-salt sediments (at least 5 km thickness may be estimated with Vp = 5 km/s). The chaotic irregular reflections within the basement high are consistent with the SDR reflections observed in A and C. The profile shown in section G crosses the tip of the Yucatan continental block (see Fig. 1 for location); it illustrates the thickening of the post-salt Jurassic section to the northeast as well as the basement high at the crossing point with the line shown in section A, which divides the pre-salt basin into two compartments.

The crustal architecture of the Gulf of Mexico remains poorly understood. Several authors who define the boundary between oceanic and continental crustal domains (OCB) for the study area (Fig. 1, also in Eagles et al., 2015; Hudec et al., 2013) referred to this boundary as the Limit of Oceanic Crust in their paper using proprietary seismic data. Christeson et al. (2014) used tectonic restoration methods constrained by refraction profiles in the northern Gulf of Mexico, while Nguyen and Mann (2016) analyzed gravity data from Sandwell et al. (2014). The OCB published by Pindell et al. (2016) was constrained by proprietary magnetic data. As shown in Figure 1, these boundaries vary dramatically in the study area, differing by as much as 75 km. Although the authors agree with Eagles et al. (2015) in that approximating the OCB with a single line is clearly an oversimplification, the

observed disagreement of 75 km between different models results from using only one method and does not represent the uncertainty of the OCB.

Using proprietary seismic data, Hudec and Norton (2019) arrived at strikingly different tectonic histories of the Yucatan and Campeche salt basins. Their study focused on the period immediately after the salt deposition and concluded that the Yucatan salt basin in the north experienced an unconfined seaward flow of salt and its cover during basin opening. In contrast, the Campeche salt basin did not experience the salt flowage. However, Hudec and Norton (2019) suggested that the crustal type underlying the seaward margins of both salt basins was "of only secondary importance." The authors defined an "outer trough" immediately adjacent to the oceanic crust (yellow polygon in Fig. 1) that is underlain by the crust of "unknown nature". That region is coincident with the "zone of uncertain crustal type" in Curry et al. (2018). This study aims to better define the location of the OCB, as well as to study the variations in the crustal architecture along the margin using all available geophysical and geological datasets, namely reflection and refraction seismic, potential fields, and well data.

This paper also will examine the presence of the seaward dipping reflectors (SDR, see Planke et al., 2000 for a general overview) on the Yucatan passive continental margin. The set of prominent SDRs is imaged in several recently published seismic data (Williams-Rojas et al., 2012; Saunders et al., 2016; O'Reilly et al., 2017; Steier and Mann, 2019; Hudec and Norton, 2019). However, Hudec and Norton (2019) imply that this zone with pronounced seaward dipping reflectors is mostly filled with the synrift sedimentary sequence rather than a series of stacked volcanic flows, although they do not rule out a volcanic origin completely. In the northeastern Gulf of Mexico, Imbert and Phillippe (2005) outlined a similar SDR province from seismic and magnetic data; it was also mapped from seismic reflections by Eddy et al. (2014), as shown in Figure 1. Both Imbert and Phillippe (2005) and Eddy et al. (2014) interpreted that feature as a volcanic SDR complex, while Curry et al. (2018) proposed an alternative interpretation for the sequence, which did not invoke volcanics. Alternatively, an integrated analysis of seismic and potential fields of Liu et al. (2019) in the northeastern Gulf of Mexico concluded that this zone is filled with dense and highly magnetic rocks, overall supporting the volcanic origin of the SDR sequences. This study will examine various scenarios for the region with visible SDRs in seismic data in the southern Gulf of Mexico (Fig. 2).

1.1. Data

An integrated geophysical approach in data analysis (Filina et al., 2019) was utilized to overcome the challenge of seismic imaging beneath the salt, i.e., to study the pre-salt sediments and the underlying crustal units. The following datasets were integrated in this study:

(1) Seismic profiles from Williams-Rojas et al. (2012) shown in Figure 2A, D, and E served as frameworks for three integrated geophysical models developed in this study. These depth-migrated seismic sections provided constraints for sedimentary layers from the seafloor to the basement.

(2) Published gravity and magnetic grids from Sandwell et al. (2014) and Meyer et al. (2017) are shown in Figure 3. The original Free-Air gravity (with a sampling interval

of 1 arc-minute, approximately 1.84 km in the study area) and Total Magnetic Anomaly grids (sampling interval of 2 arc-minutes) were gridded using 2 and 4 km sampling intervals, respectively. The series corrections were applied to both fields before spatial analysis (described in detail in the Spatial Analysis of Potential Fields section).

(3) Vintage seismic refraction data from Ewing et al. (1960) and Ibrahim et al. (1981), shown as white circles in Figures 1 and 3, were used as constraints for the depth to Moho boundary. Most of these points are on oceanic crust, suggesting that the depth to the Moho shallows from 19 to 16 km toward the continent. In the continental domain, only two points have refractions from the Moho over a thinned continental crust (the most eastward points in Figs. 1 and 3), suggesting that the base of the crust is between 23.4 and 29.6 km (Ewing et al., 1960).

(4) Physical properties (densities and magnetic susceptibilities) of the sedimentary section and the upper crustal rocks are constrained by various wells in the Gulf of Mexico (Hilterman, 1998; Buffler et al., 1984) and previous models (Miranda-Peralta et al., 2014; Filina et al., 2015; Liu et al., 2019; Filina, 2019). More details on the physical properties is provided in the Integrated Geophysical Modeling section.

(5) Bathymetry data from the General Bathymetric Chart of the Oceans (GEBCO) from Weatherall et al. (2015) was used to extract the water bottom horizon for the models. The original grid with a 30 arc-seconds sampling interval (approximately 0.92 km in the study area) was gridded with a 1 km cell size.

(6) Several published seismic cross-sections were used as constraints during the modeling. The profile from Hudec et al. (2013) shown in Figure 2B illustrates the "outer trough." Understanding the nature of the crust beneath this zone was one of the objectives for Model 1. The cross-section from O'Reilly et al. (2017) shown in Figure 2C was also used to confirm the region with the SDRs included in that model. The location of both lines in Figure 2B and C were not explicitly described in the original papers; however, sedimentary structures suggest that these lines are in the proximity of the modeled Line 1 from Williams-Rojas et al. (2012; Fig. 2A). The lines from Miranda-Peralta et al. (2014) and Horn et al. (2017) shown in Figure 2F and G, respectively, were used to validate variations in the thickness of the pre-salt sediments as well as in the post-salt Jurassic section. These two profiles are strike lines crossing the margin (see Fig. 1 for location); they were not modeled, as the variations in the out of plane geological structures challenge the 2D assumptions of the modeling. The cross-section of Miranda-Peralta et al. (2014) in Figure 2F (in two-way traveltime) shows the pre-salt sediments up to 2 s thick, which corresponds to an estimate of 5 km assuming a compressional seismic velocity of 5 km/s for these old and compacted sediments (Telford et al., 1990). This value was used as an upper bound for the thickness of pre-salt sediments during the modeling. The strong irregular reflections within the basement high of the two-way travel time seismic section in Figure 2F correlate with the SDRs observed in the crossing lines (Fig. 2A and C), therefore increasing the confidence of the interpreted SDR province crossed by Model 1. The cross-section from Figure 2 of Horn et al. (2017) (not shown here) was also used to constrain the depth to Moho at the eastern

(landward) sides of Models 2 and 3 as being approximately at 35 km, as well as to justify the presence of the intrusive bodies in the lower continental crust.

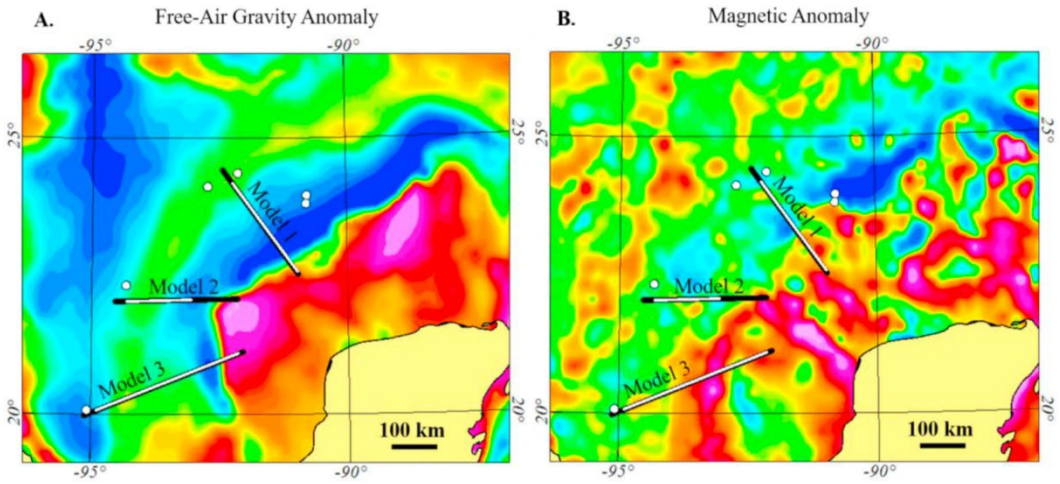

Figure 3. Potential fields used for the study. (A) Free-Air gravity (Sandwell et al., 2014), (B) Magnetic anomaly (Meyer et al., 2017). The black lines show three integrated geophysical models developed in this study, the white segments indicate the extents of seismic cross-sections from Figure 2. The white dots are vintage seismic refraction data from Ewing et al. (1960) and Ibrahim et al. (1981).

2. Methods

2.1. Integrated geophysical modeling

Three integrated geophysical models were developed (Figs. 4–7). The models consist of multiple layers in the subsurface from sea level (0 km) to 40 km. The physical properties of the rocks in each layer, namely density and magnetic susceptibility, were assigned based on known or assumed rock types. The equivalent rock units in all three models share the same physical properties. The gravity and magnetic responses of each model were then computed using the GM-SYS module of Oasis Montaj (in assumptions of isostatic compensation and absent remnant magnetization) and compared with the observed potential fields extracted from the grids shown in Figure 3. To account for the insufficient resolution of the observed satellite gravity data for shallow, short-wavelength structures, the computed gravity field was low-passed filtered using a 50 km wide Gaussian window. The subsurface model was then adjusted in order to agree with seismic reflection data, obey all the constraints (i.e., refraction data), provide a reasonable fit in both potential fields, and remain geologically sound. Below is a detailed description of each modeled layer along with all the constraints imposed on both physical properties and on geometry (i.e., depth and thickness).

- Water is the topmost layer and it is the best-known one. It was constrained by the bathymetry data from Weatherall et al. (2015) and kept unchanged during the

modeling. The density of water was assumed to be 1.03 g/cm^3 (Telford et al., 1990); zero magnetic susceptibility was assigned to this layer.

- The sedimentary section was split into five layers, ranging from the most recent and the least dense (2.25 g/cm3) sediments to the densest pre-salt sedimentary section with an assumed density of 2.6 g/cm^3. Though the authors were not able to find the published density logs for wells in the study area, the assigned density values for the post-salt sediments are consistent with similar studies in the northern Gulf of Mexico (Filina, 2019; Liu et al., 2019). These assigned densities for the sedimentary section agree very well with the values derived for the Yucatan margin by Miranda-Peralta et al. (2014; their Fig. 3). All post-salt sedimentary layers were assumed to be nonmagnetic. The pre-salt sedimentary section may include sediments ranging in age from Permian to middle-Jurassic and most likely contains some portion of Triassic-Jurassic red beds associated with the continental rifting stage (Miranda-Peralta et al., 2014). As no published magnetic susceptibilities of the pre-salt section were available, magnetic susceptibility of 500 μcgc [microcgs] ($6.3{\cdot}10^{-6}$ SI) was assigned to what are assumed to be slightly magnetic red beds (Hunt et al., 1995).
- The stretched and thinned continental crust was split into the upper and lower crustal units. This is consistent with the overall crustal structures in the northern Gulf of Mexico (Filina, 2019; Liu et al., 2019) constrained by much better-quality refraction data of the GUMBO experiment (Eddy et al., 2014, 2018; Christeson et al., 2014). The upper continental crust of the Gulf of Mexico was penetrated only in the eastern Yucatan margin in Deep Sea Drilling Program (DSDP) Leg 77 (Buffler et al., 1984, inset map in Fig. 1). The well at site 538A sampled the metasedimentary rocks of Cambrian age intruded with Jurassic diabase dikes. The average density value for these rocks (2.78 g/cm^3) was assigned to the modeled upper crust. A slightly denser value of 2.8 g/cm^3 was used for the SDR province crossed by Model 1. As the Curie depth in the study area varies from 20 to 30 km (Li et al., 2017), both crustal layers were assumed to be magnetic. The magnetic susceptibilities of the crustal rocks from the site 538A (Buffler et al., 1984) were used to estimate 1500 μcgc ($19{\cdot}10^{-3}$ SI) for the upper continental crust and 2500 μcgc ($31{\cdot}10^{-3}$ SI) for the SDR province identified along the modeled line 1. The lower continental crust was assumed to have a density of 2.9 g/cm^3, which is consistent with the values reported in Christensen and Mooney (1995). The magnetic susceptibility of the lower continental crust cannot be constrained with the well data, so it was assumed to be 4200 μcgc ($53{\cdot}10^{-3}$ SI); this value is within the range published by Hunt et al. (1995). Several intrusive bodies were identified within the lower continental crust. Their magnetic susceptibility was assigned to 8000 μcgc ($100{\cdot}10^{-3}$ SI), and their density was assumed to be 2.95 g/cm^3, consistent with similar studies in the northern Gulf of Mexico (Filina, 2019; Liu et al., 2019).
- The oceanic crust consisting of two layers was assumed based on the synthesis model of Christeson et al. (2019). The top of the oceanic crust, i.e., oceanic layer 2 composed of basalts, was assigned a density of 2.65 g/cm^3 (Carlson and Herrick,

1990) and magnetic susceptibility of 2200 μcgc ($28 \cdot 10^{-3}$ SI) (Hunt et al., 1995). The lower layer of oceanic crust—gabbroic layer 3—was assigned a density of 2.85 g/cm^3 (Carlson and Herrick, 1990) and magnetic susceptibility of 5000 μcgc ($63 \cdot 10^{-3}$ SI, Hunt et al., 1995). The thickness of oceanic crust and depth to the Moho was constrained with seismic refraction data from Ewing et al. (1960) and Ibrahim et al. (1981), shown as white circles in Figures 1 and 3.

- The mantle was assumed to have a density of 3.3 g/cm^3 and zero magnetic susceptibility (Telford et al., 1990).

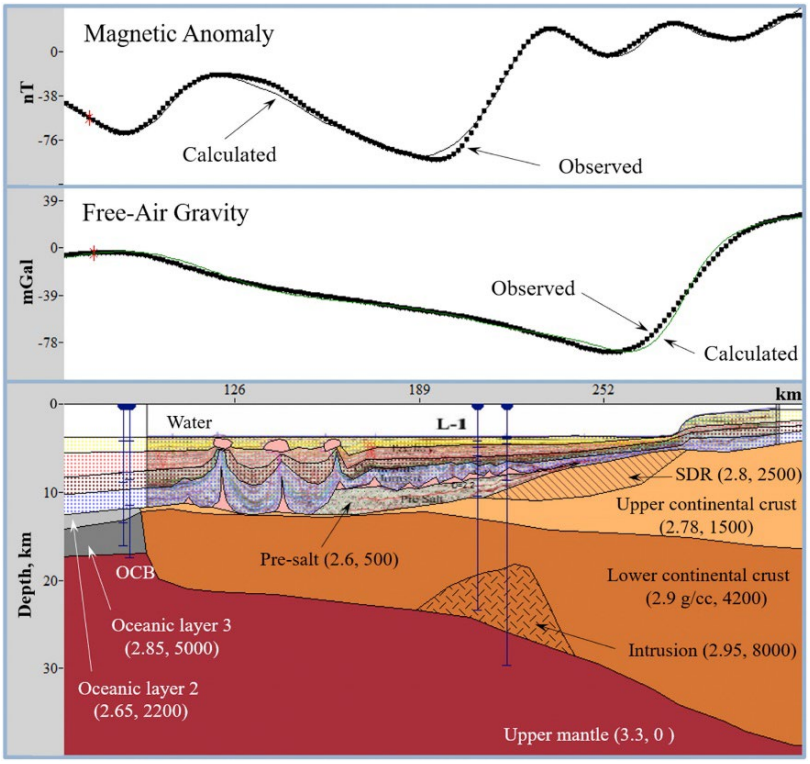

Figure 4. The preferred version of the Model 1. In this model, the good match between observed and computed magnetic (top panel) and gravity (middle panel) signals is achieved. The observed and computed potential fields are tied over the oceanic domain (red stars). The geological model (bottom panel) is constrained with vintage refraction data (dark blue marks show the projections to the modeled profile, see Fig. 1 for location). The numbers in the parentheses are the densities in g/cm^3 and magnetic susceptibilities in μcgc. Vertical exaggeration is 3.

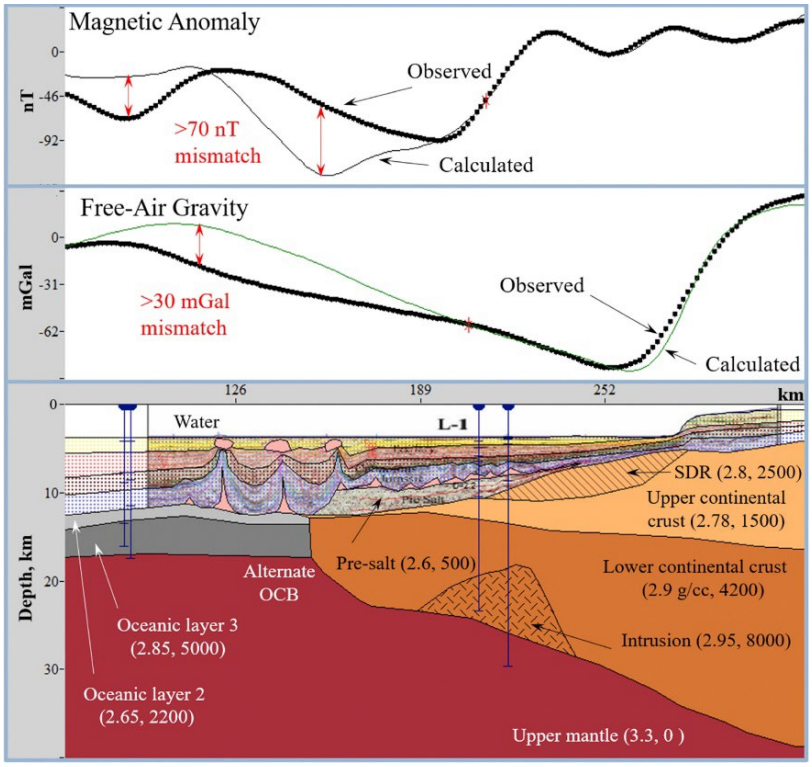

Figure 5. The alternative scenario for Model 1—the oceanic crust beneath the outer trough. In this scenario, the large mismatches are observed in both fields. Vertical exaggeration is 3.

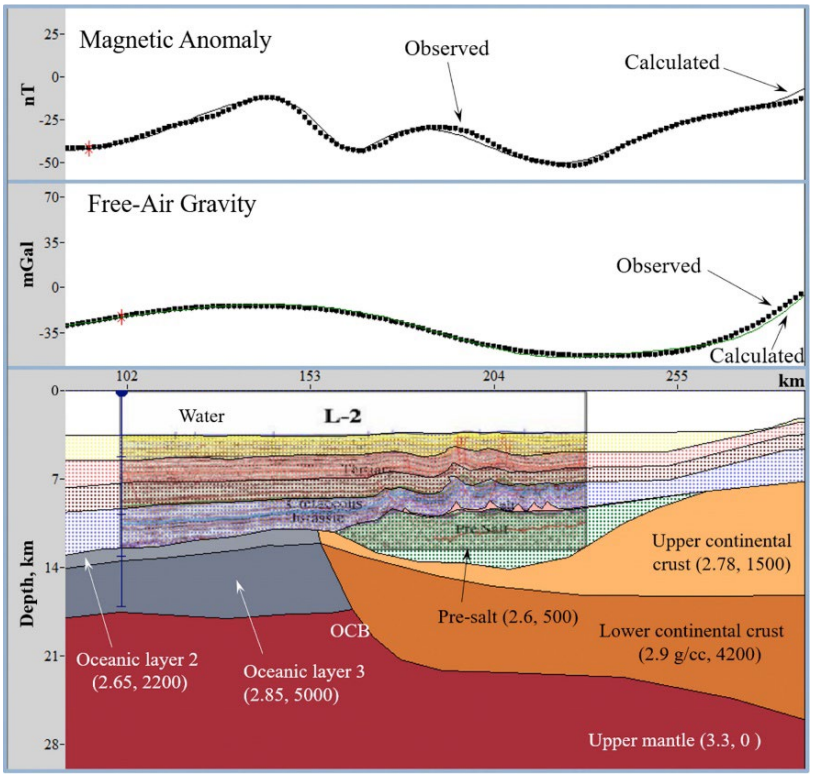

Figure 6. Model 2; see the caption to Figure 4 for details. Vertical exaggeration is 3.5.

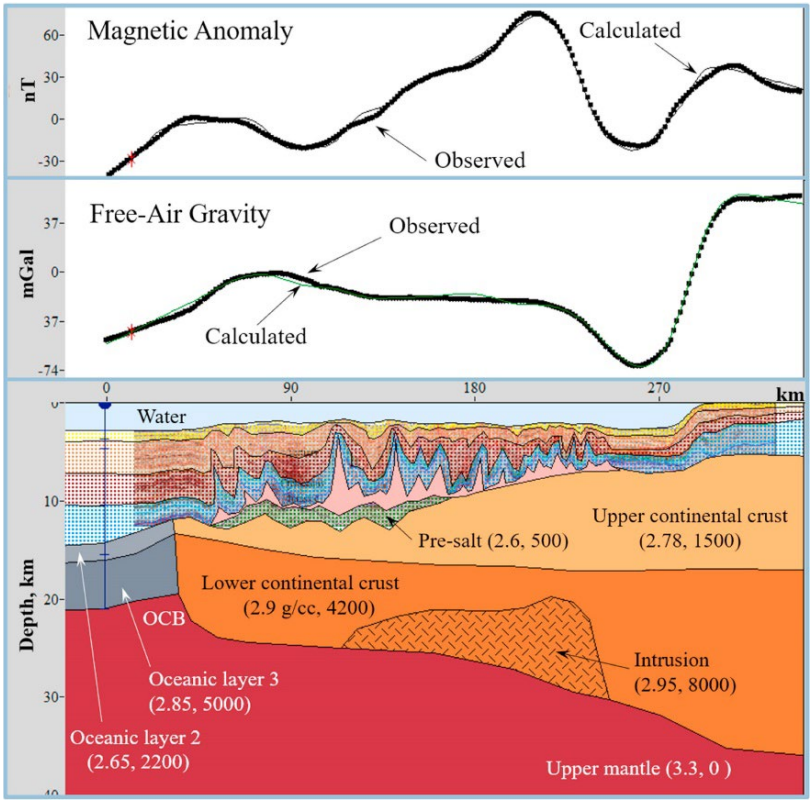

Figure 7. Model 3; see the caption to Figure 4 for details. Vertical exaggeration is 4.0.

2.2. Spatial analysis of potential fields

Observed potential fields—gravity and magnetic (Fig. 3)—comprise the cumulative signals of rocks with different physical properties in subsurface. Gravity responds to lateral variations in rock density while magnetic anomalies to the contrasts in their magnetic susceptibility. Major geological structures in the study area associated with noticeable contrasts in both physical properties include the water/sediments interface (i.e., bathymetry), salt bodies in the sedimentary section, the pre-salt basin and the SDRs within the upper crust, the boundary between oceanic and continental crustal domains (i.e., OCB) and the crust-mantle interface (i.e., the Moho). The former one—the effect of water over the sediments—is negligible in magnetics, while it is significant in gravity and has to be accounted for via Bouguer correction (Telford et al., 1990). The salt/sediments contrasts correlate to the shortest wavelengths in the gravity field due to relatively narrow widths of salt diapirs and keels; their signatures are negligible in magnetics because of a very low magnetic susceptibility contrast of salt with sedimentary rocks. In contrast, the effect of the deepest subsurface interface—the Moho—is associated with a broad regional anomaly that can be removed via filtering. Therefore, to highlight the effects of the sources within the crust and of the contact between oceanic and continental crusts (OCB), a series of transformations to both potential fields was applied, as is described below.

In gravity, the Bouguer correction was computed with the densities of water and the top sediments of 1.03 g/cm^3 and 2.25 g/cm^3, respectively. The regional trend in the Bouguer gravity anomaly (i.e., the effect of deep sources, like the Moho boundary) was computed via upward continuation to an elevation of 40 km. This value was chosen by trial and error as the one that removes high-frequency components in gravity due to shallower subsurface structures and results in the broad and smooth signal from deep regional sources. Once the regional trend was computed, it was subtracted from the Bouguer gravity field. The tilt derivative filter (Salem et al., 2008) was then applied to the residual gravity anomaly (i.e., with removed water signal and regional trend) in order to highlight the regions where gravity changes the most (Fig. 8A).

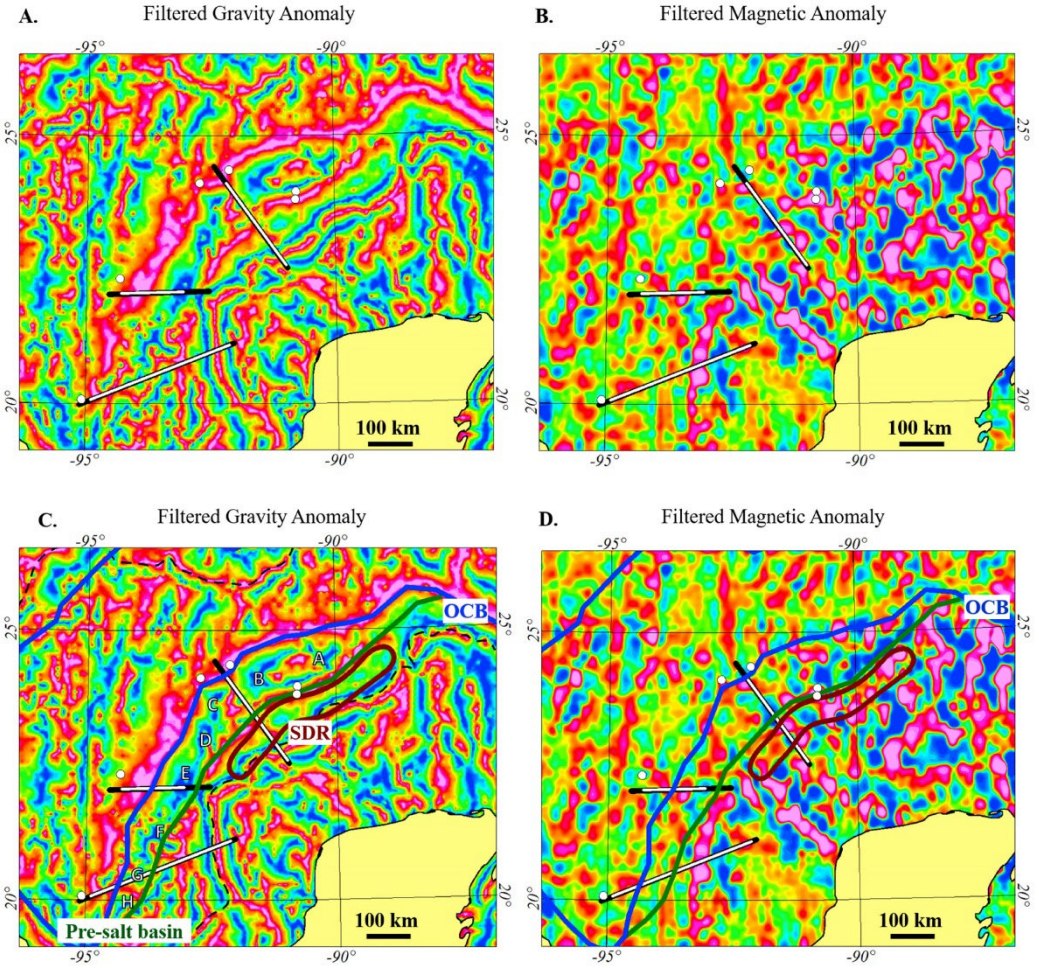

Figure 8. Filtered potential fields: (A) Tilt derivative of the residual Bouguer gravity, (B) First vertical derivative of the residual Reduced to Pole magnetic, and (C, D) interpreted tectonic zones. The dashed black line in (C) marks the shelf break that is associated with the sharp change in bathymetry that is evident in filtered gravity data.

In magnetics, the reduction to the pole (RTP) transformation was performed (with an inclination of 54° and a declination of 7°) to remove a skewness of the magnetic anomalies due to a nonvertical ambient field. These ambient magnetic field parameters were inferred based on the date of magnetic surveys in the southern Gulf of Mexico (Meyer et al., 2017). The regional trend of the RTP magnetic field was also computed via upward continuation but to a lower elevation of 20 km, as the magnetic field decreases faster with distance than gravity (Telford et al., 1990). Once the regional trend was removed, we applied the first vertical derivative filter to the residual magnetic field to further highlight the effects of geological structures. The result is shown in Figure 8B.

3. Results and discussion

3.1. Model 1—the Yucatan sub-basin

Model 1 (Fig. 4) crosses the central part of the Yucatan salt basin. The most intriguing feature of that region is the drop in the basement of at least 2 km at the northwestern end of the model, adjacent to the OCB, that Hudec and Norton (2019) refereed as an "outer trough" (Fig. 2 A, B, and C). This feature is about 40 km wide along Model 1. The nature of the crust beneath this feature is unknown (Curry et al., 2018; Hudec and Norton, 2019), and the location of the Ocean-Continent contact varies within 40 km among the published models (Figs. 1 and 2A). Two possible scenarios for crustal affiliation beneath the outer trough are illustrated—continental (Fig. 4) and oceanic (Fig. 5). Four vintage refraction points were used to constrain the depth to the Moho; two of them were projected from 100 km away (see Fig. 1 for location).

Model 1 (Fig. 4) suggests that the crustal thickness varies from > 30 km at the beginning of the line to ~5 km in the oceanic crust at the northwestern end of the line constrained by the vintage refraction data (Ewing et al., 1960). The crust beneath the outer trough is extended continental with a total thickness of ~10 km (Fig. 4). However, the distribution of the individual crustal units implies the conditions close to the exhumation of the lower continental crust, presumably during the final stage of rifting (i.e., post-salt as in Hudec et al., 2013). A similar crustal organization may be interpreted in the refraction data (Eddy et al., 2014; Christeson et al., 2014) on the conjugate northeastern Gulf of Mexico margin (Lundin and Dore, 2017; Beutel and Filina, 2020). The profile GUMBO4 (Christeson et al., 2014) shows ~10 km thick and ~50 km wide continental crustal block with high velocity (Vp ~7 km/s) adjacent to the interpreted OCB that is consistent with exhumed lower continental crust. Alternatively, this region of fast seismic velocities may be interpreted as an oceanic crust or heavily intruded, magmatically altered continental crust. Both alternative scenarios will be addressed below.

The boundary between oceanic and continental crustal domains is marked by a pronounced trough in observed magnetic signal and with a distinct high in gravity (Fig. 4). A lateral shift of this boundary of more than a few kilometers results in a rapid deterioration in fit for both potential fields. The pre-salt section along Model 1 is up to 3 km thick, which is consistent with figure 5 of Miranda-Peralta et al. (2014). Williams-Rojas et al. (2012), Figure 2A, interpreted this section to comprise at least two sequences; these were merged into

one pre-salt layer during modeling (Fig. 4), as a rather negligible contrast in physical properties was inferred between them.

Another intriguing feature of this model is an apparent thickening of the post-salt Jurassic section that can be also observed in Figure 2C. Williams-Rojas et al. (2012) interpreted a relatively thin post-salt Jurassic section over the outer trough—this can be inferred from the Cretaceous (blue) horizon in Figure 2A that is indicated with a black arrow and labeled with "K." In contrast, the cross-section of O'Reilly et al. (2017) shown in Figure 2C suggests that the post-salt Jurassic section over the outer trough is much thicker. This apparent thickening of this section is also evident from two orthogonal seismic lines, shown in Figure 2 F and G. The post-salt Jurassic sequence is absent at the edge of the carbonate platform; it is approximately 2 km thick above the pre-salt basin in the central part of Model 1 and approximately 3.5 km over the outer trough (Fig. 2 A and G). The model in Figure 4 shows that the thickened Jurassic section of the outer trough rests immediately on the acoustic basement, i.e., not underlain by pre-salt sediments. This is consistent with Hudec and Norton (2019), who outlined the outer trough region (yellow polygon in Fig. 1) of two zones separated by a horst block. They did not identify any pre-salt sediments beneath the outer trough, although this may be due to obscured seismic image. Model 1 crosses the outer trough over that horst block, so the salt rests directly on the acoustic basement (Fig. 4). This narrow basement high is also evident in the crossing line of Horn et al. (2017) shown in Figure 2G.

Model 1 includes the region of SDRs in the upper crust (Fig. 4) with an elevated density and higher magnetic susceptibility. For gravity, the density contrast between SDR rocks and the upper continental crust is not crucial (i.e., the mismatch in gravity could be worked out if no SDR is included in the model). In contrast, the SDR complex is necessary to satisfy the magnetic signal, as it demands the presence of rocks with elevated magnetic susceptibility. If no SDR is included in the model, the observed magnetic pattern over that region, i.e., a trough—bump pattern between the ranges of 200 and 300 km—will not be matched. The series of irregular reflectors in the basement high of the line in Figure 2F (strike line), combined with the strong reflectivity at the southern end of the pre-salt section seen in Figure 2 A and C (dip lines), further support the SDR province in Model 1. The SDRs on the Yucatan margin are also imaged in seismic sections published by Saunders et al. (2016), Steier and Mann (2019), and Filina et al. (2020a). A similar SDR complex, also aligned with a strong magnetic anomaly, is also interpreted in the northeastern Gulf of Mexico (Imbert and Philippe, 2005; Eddy et al., 2014; Liu et al., 2019; see location in the inset map in Fig. 1) that represents the conjugate margin to the study area (Lundin and Dore, 2017; Beutel and Filina, 2020).

A large magnetic intrusive body in the lower crust is also required in order to explain a pronounced magnetic anomaly in the central part of Model 1 (Fig. 4) that was interpreted as evidence of magmatism during the Triassic-Jurassic continental rifting stage. Similar intrusive bodies are interpreted at the conjugate northern Gulf of Mexico margin from seismic refractions (Eddy et al., 2014, 2018; Christeson et al., 2014). In profile GUMBO4 (Christeson et al., 2014), the interpreted intrusive body (Vp ~7.5 km/s) is located landward of the high-velocity region, presumably of exhumed lower continental crust, just like an intrusive body in Figure 4. An integrative analysis of those structures in the northern part of the

basin (Filina, 2019; Liu et al., 2019) suggests that they require high densities and magnetic susceptibilities to explain observed potential fields. In the southern Gulf of Mexico, no comprehensive refraction data exist, but these intrusive bodies in the lower continental crust are interpreted from seismic reflection data (Horn et al., 2017). Moreover, the evidence of magmatic addition during the rifting stage of the basin opening was documented from the DSDP drilling (Leg 77, Fig. 1), as described above. Therefore, the strong magnetic signal in the central part of Model 1 was modeled as a superposition of the SDR complex with a feeding intrusive body in the lower crust that is positioned basinward of the SDR complex (Fig. 4). However, due to known nonuniqueness of the potential fields modeling, alternative interpretations—i.e., a single intrusive body of irregular rugose shape within a lower crust with no magnetic SDR complex—could also be modeled. However, we consider this scenario less likely, as SDR are evident in seismic, aligned with pronounced magnetic anomalies, interpreted on the conjugate margin, and consistent with the basement samples from DSDP well.

The observed and computed potential fields were tied over the oceanic domain (shown with red stars in Fig. 4), where the model is least complex and best constrained with refraction data (see Fig. 1 for locations of refraction points). Overall, the modeling resulted in a good match for both potential fields. Two alternative geological scenarios were also tested. The first one—oceanic crust beneath the outer trough—is shown in Figure 5. This scenario results in an enormous (exceeding 30 mGal) misfit in gravity. This mismatch demands lower density rocks in the subsurface and would not be not balanced even if the entire sedimentary section between the basement and the Cretaceous horizon is filled with salt. Magnetic signal also shows a dramatic mismatch, which combined with an unresolvable misfit in gravity disproves this geological scenario. The second alternative scenario (not shown) assumes that the crust beneath the outer trough is of magmatic origin, i.e., has physical properties similar to the intrusive body shown in Figures 4 and 5. In this case, the moderate gravity mismatch of ~10 mGal is observed that can potentially be worked out with increased crustal thickness. However, this scenario results in a large > 150 nT magnetic misfit that cannot be resolved without reducing magnetic susceptibilities to the values of the lower continental crust, i.e., eliminating a magmatic addition. Therefore, this scenario is also not feasible with observed potential fields.

3.2. Model 2—the northern part of the Campeche sub-basin

The second model (Fig. 6) is aligned with the seismic reflection section L-2 of Williams-Rojas et al. (2012) shown in Figure 2D. The seismic profile does not cross the region with potential SDRs, so the presence or absence of that zone cannot be confirmed with seismic data. In the magnetic field, there is a strong positive Campeche magnetic anomaly to the south of this line (Fig. 3B). Another strong positive southeast trending anomaly is just off the landward edge of the profile. A magnetic fit for preferred Model 2 (Fig. 6) was achieved without introducing any igneous bodies, such as SDR or crustal intrusives.

The oceanic crust is constrained with point 4E of Ibrahim et al. (1981) that is located 30 km to the north at the oceanward end of the line (Fig. 1). The OCB is coincident with the edge of the folded sedimentary section and agrees with the location of Hudec et al. (2013) for this line.

In gravity, a good regional fit was achieved suggesting somewhat similar to the previous model structure of the extended continental crust—the thickness is ~10 km, while the upper crust is dramatically thinned. In contrast to Model 1, this thinned continental crust is overlain by up to 5 km thick pre-salt sedimentary section that is partially imaged in seismic reflection data (Fig. 2D).

3.3. Model 3—southern part of the campeche sub-basin

The last model (Fig. 7) is constrained with the seismic reflection profile L-3 of Williams-Rojas et al. (2012) shown in Figure 2E. This model crosses the region with a significantly greater volume of salt with respect to the other two lines. The sedimentary section comprises multiple folded and faulted strata related to salt tectonics. The salt resides primarily in the cores of the folds within the sedimentary column. Although the pre-salt sediments are labeled in seismic, the base of that section (i.e., basement boundary) is not interpreted within the pre-salt basin (Fig. 2E).

The modeling suggests much thinner pre-salt sediments (not exceeding 2 km) with respect to other lines. The crust beneath the presalt is interpreted to be stretched continental with a total thickness ranging from 16 to 11 km (Fig. 7). According to the model, the OCB is adjacent to the outer edge of the folded strata. The oceanic crust at the southwestern end of the line was constrained by the seismic refraction point 5S from Ibrahim et al. (1981), fixing the depth to Moho at 21 km (Fig. 7). The convex shaped sedimentary section above the interpreted oceanic crust suggests OCB coincident with a basement high; this crustal architecture is also demanded by gravity and magnetic signals (Fig. 7).

This model crosses the large-amplitude magnetic anomaly (Campeche magnetic high, Fig. 3B), suggesting that at least one large anomalous body with a large susceptibility contrast is necessary to explain the observed magnetic signal. The model in Figure 7 shows one magnetic intrusion at the base of the crust with the same magnetic susceptibility as that in Model 1. As the solution of magnetic modeling is nonunique, other possible scenarios for the anomalous magnetic source(s) were evaluated.

The above-salt sedimentary section is imaged relatively well in seismic reflection data (Fig. 2E) and does not show any voluminous igneous intrusives that can be responsible for the observed magnetic anomaly. The pre-salt section, even if assumed to be magnetic with the highest possible magnetic susceptibility for sedimentary rocks, will produce a magnetic signal of several orders of magnitudes less than the observed one. Alternatively, the source of the magnetic signal could be placed at the top of the crust (similar to the SDRs in Model 1). However, in this scenario, the hypothetical SDR complex would have unrealistically high magnetic susceptibility i.e., the rocks with such dramatic susceptibilities do not exist. Another scenario could use several anomalous bodies (again, similarly to Model 1—a deep intrusive body "feeding" an SDR complex), but this model was also rejected for two reasons. First, the lack of the SDRs in seismic, although they may be not well imaged because of the overlying salt. Second, the observed magnetic signal is a pronounced trough, while the SDR complex in Model 1 correlates to a magnetic high. Therefore, the observed high-amplitude magnetic signature agrees better with one strongly magnetic anomalous body of significant volume (as shown in Fig. 7). However, it could also be possible to fit

the observed magnetic signal with several stacked magnetic bodies within the crust. These two options are not distinguishable from magnetic modeling alone.

3.4. Spatial analysis

The three models (Figs. 4, 6 and 7) allowed mapping the locations of the major tectonic features, namely the OCB, the edge of the pre-salt basin, and the overall extent of the SDR province. These structures show apparent correlation with the lineaments observed in filtered potential fields (Fig. 8): The OCBs from all three models are associated with the same gradient along the edge of the dramatic gravity high. In magnetics, it corresponds to a general break in anomalies' character. All three models suggest that the pre-salt basin corresponds to an overall gravity low. The eastern boundary of the pre-salt basin can be easily mapped in both gravity and magnetic fields. The variations within the filtered gravity (Fig. 8C) also suggest the variations in the thickness of the pre-salt section, implying compartmentalization of the pre-salt basin. The major compartments are labeled A through H in Figure 8C.

3.5. Modeling uncertainties

It is well known that the solution of an inverse problem of any potential field is not unique (i.e., multiple models can fit the same observed signal). This nonuniqueness arises from the fact that an observed signal is a function of the two major unknowns within the model—the physical properties and the geometry (depth and thickness). In theory, both the depth of modeled horizons and the physical properties can be adjusted in order to modify computed gravity or magnetic signals. Therefore, if no prior knowledge about these parameters exist, there is an infinite number of solutions for potential fields. If some of the modeled parameters—either physical properties or geometries—are constrained (i.e., fixed during the modeling), the number of solutions decreases dramatically toward a range of possible models that can fit an observed field.

For the models in Figures 4, 6, and 7, multiple constraints were imposed both on physical properties (densities of sedimentary section and the upper crust were fixed) and on geometries of modeled layers (seismic reflections and refractions). Some parameters simply must be assumed based on literature (such as physical properties of the mantle rocks). Moreover, the physical properties derived during the modeling, namely density and magnetic susceptibility of the crustal layers, must be the same for the corresponding rocks of all three models, imposing additional restrictions on the modeling process. The geometries derived from modeling, such as depths and thicknesses of the crustal blocks, should not only agree with seismic constraints but also should not have erratic geometries to be geologically valid. The preferred models (Figs. 4, 6, and 7) represent the best (and the simplest) solutions for the three lines used in the study with all available constraints and assumptions.

The fact that we map our tectonic boundaries based on the lineaments seen in both fields (Fig. 8) boosts the overall confidence of our interpretation. Below we describe major tectonic features that were targeted in this study.

3.6. Crustal architecture

Three integrated geophysical models illustrate the changes in the crustal architecture along the margin. The oceanic crust is thinner in the north (5 km, Models 1 and 2) than in the south (7 km, Model 3). This is constrained with vintage refraction data (see locations in Figs. 1 and 3) and with known variations in the oceanic crust of the northeastern Gulf of Mexico imaged by the GUMBO refraction experiment (Eddy et al., 2014; Christeson et al., 2014). These variations in the thickness of oceanic crust are interpreted by Filina et al. (2020b) to represent the two episodes of oceanic spreading—the initial one (older, Jurassic) that produced the thinner crust (~5 km), while the younger one (late Jurassic to early Cretaceous) produced thicker crust (up to 9 km). The thinner oceanic crust adjacent to the Yucatan basin (Models 1 and 2) is consistent with the older spreading episode, while the thicker oceanic crust adjacent to the Campeche salt basin (Model 3) is interpreted to be younger, which is also consistent with a tectonic reconstruction of Beutel and Filina (2020).

The continental domain clearly comprises two distinct crustal provinces: the zone of thinned and stretched crust (~10 km thick) immediately adjacent to the OCB and much thicker (> 30 km) crust beneath the carbonate platform that appears to be barely affected by the rifting process. The crust in the former zone is composed of two layers: the upper continental crust varying in thickness from almost 0 to 7 km (Model 3) and the lower crust up to 10 km thick beneath the outer trough. Models 1 and 2 suggest the conditions close to the exhumation of the lower crust in the continental domain adjacent to OCB (Figs. 4 and 6). The region of the nearly removed upper continental crust coincides with the zone of the thicker post-salt Jurassic sediments that are seen in seismic data (Fig. 2 C, F, and G). The inferred region of the Jurassic post-salt thickening is shown in Figure 1 with a white dotted outline; it appears to be generally coincident, although slightly wider than the outer trough identified by Hudec and Norton (2019) in the northern part of the Yucatan salt basin. This thickening of the post-salt Jurassic section implies that this region was a local depocenter during the time between the end of salt deposition and the initiation of the oceanic spreading. We postulate that the removal of the upper crust inferred from our modeling (Figs. 4 and 6) occurred in the latest, post-salt stage of continental rifting. This removal of a relatively light layer resulted in the subsidence of the denser lower crust before the oceanic spreading initiated. This subsidence not only provided accommodation space for post-salt Jurassic sediments (as seen in Fig. 2) but also caused the unconfined seaward flow of salt and its cover as described by Hudec and Norton (2019). In contrast, no rift-related withdrawing of the upper continental crust, and consequently no exhumation of the lower continental crust, is concluded for the adjacent Campeche basin (Model 3). The crust beneath that basin is thicker (> 10 km) and has a much thicker layer of the upper continental crust. This is also consistent with the absence of the salt-detached Jurassic translation concluded by Hudec and Norton (2019).

3.7. Ocean-continent boundary

The contact between continental and oceanic rocks is associated with a significant contrast in physical properties of these rocks. The three integrated models (Figs. 4, 6, and 7) show that this boundary corresponds to signals in both potential fields—a pronounced high in gravity and a high-trough pattern in magnetics. In the spatial analysis, all three modes show

that OCB correlates with the edge of the dramatic gravity high (Fig. 8C) that corresponds with a change in character in filtered magnetics (Fig. 8D). This correlation permits tracing the OCB outside of our seismic coverage. Overall, the spatial analysis of potential fields, constrained with three integrated geophysical models, results in a more confident location of the Ocean-Continent Boundary than the previous studies (see the variations in Fig. 1 and the marked discrepancies in Fig. 2).

3.8. Pre-salt basin

The pre-salt basin extends along the eastern margin of the Yucatan peninsula. It is up to 70 km wide in the southern part of the Campeche sub-basin (to the south of Model 3), widens up to 100 km under the Yucatan salt province and pinches out to the north of Model 1 (Fig. 8 C and D). According to filtered gravity, the pre-salt basin appears to be compartmentalized with a series of generally N–S trending basement highs (Fig. 8C). Four major compartments correlating with gravity lows can be identified beneath the Yucatan salt basin (labeled A through D in Fig. 8C). The seismic line of Horn et al. (2017) crosses compartments B and C and images the basement high dividing them (Fig. 2G). This basement high corresponds to highs in both filtered gravity and magnetic fields (Fig. 8).

Four major compartments can be identified under the Campeche salt basin as well; they are named E through H in Fig. 8C. The largest one, compartment E, may be further subdivided into smaller parts (along the local gravity highs). Overall, compartment E appears to be associated with the most pronounced gravity low. It is crossed by the seismic line of Miranda-Peralta et al. (2014) shown in Figure 2G, suggesting that the thickness of the pre-salt sediments is ~5 km. The other three compartments in the Campeche sub-basin are smaller and appear to be filled with thinner sedimentary sections. This is consistent with Model 3 that shows a series of tilted crustal blocks under the pre-salt sediments; the identified compartments appear to correlate with the lows between these crustal blocks. However, the southern part of the Campeche basin hosts multiple salt structures (see the seismic cross-section in Fig. 2E) that may interfere with spatial analysis. The wavelength of the gravity anomaly due to a salt diapir is much shorter than that of the pre-salt basin. With the pre-salt compartments getting narrower to the south (i.e., compartments F, G, H), the wavelength of their gravity signal becomes shorter. This, combined with the increased volume of salt, complicates the analysis and challenges the resolution of satellite gravity data used for the study. The pre-salt compartments are less obvious in magnetic data than in gravity because the observed magnetic signal represents the superposition of multiple sources within the crust (SDRs, intrusions) of a much larger volume than the pre-salt structures. The resolution of the magnetic dataset used for the analysis, although it is sufficient for the profile modeling and for studying the large-scale geological structures, does not allow confident mapping of smaller-scale features, such as compartments in the pre-salt basin. Therefore, the interpreted structures in the pre-salt basin rely more on gravity than on magnetics.

3.9. Igneous addition

Our models suggest igneous addition within the subsurface, namely an SDR complex inferred from Model 1 and several igneous intrusions in the lower crust identified in Models

1 and 3. The crustal intrusive bodies with high seismic velocities aligned with strong magnetic signals are imaged from seismic refraction profiles in the northern Gulf of Mexico (Eddy et al., 2014, 2018; Christeson et al., 2014; Van Avendonk et al., 2015). Many authors interpret them as rift-related features (Eddy et al., 2014, 2018; Christeson et al., 2014; Filina, 2019; Liu et al., 2019), although an alternative interpretation is offered by Van Avendonk et al. (2015) for the northeastern Gulf of Mexico suggesting that these represent preexisting crustal inhomogeneities related to Permian Ouachita-Marathon orogeny that preceded the formation of the Gulf of Mexico. The origin of these structures cannot be established uniquely from the potential fields, but they require high densities and high magnetic susceptibilities to explain observed gravity and magnetic anomalies. We prefer the rift-related magmatic addition interpretation of these structures as it is consistent with the basinward dipping reflectors observed in seismic (Fig. 2) and with the results of the DSDP well to the east of the study area (Buffler et al., 1984; see inset map in Fig. 1) that encountered Paleozoic basement intruded by diabase dike with Jurassic crystallization age.

The SDRs in Model 1 are dictated by the observed magnetic anomalies. This zone is also coincident with the region of SDRs that can be interpreted in seismic data (Fig. 2 A and C). The extent of the SDR province was determined based on our spatial analysis (Fig. 8) to be up to 400 km long and up to 50 km wide. The dimensions of the SDR zone identified in the northeastern Gulf of Mexico vary between the authors—Eddy et al. (2014) suggest the extent of approximately 200 × 45 km based on proprietary seismic data, while this zone is interpreted to be slightly wider (48 km) and longer (235 km) by a similar analysis of potential fields of Liu et al. (2019). Beutel and Filina (2020) expanded the mapped SDR complex in the northeastern Gulf of Mexico to a similar extent mapped in this study; they used the mapped SDR complexes on both margins to constrain the tectonic reconstruction of the basin as these SDR complexes must be aligned at the conjugate margins.

The observed magnetic signatures demand several igneous intrusions in the lower continental crust. The intrusive bodies are modeled in two out of three lines located immediately at the boundary between the stretched and intruded continental crust and the relatively unstretched crust (> 30 km) in the east. If they are rift-related features, they support the presence of the SDR complex interpreted under the Yucatan salt basin (Model 1). However, this disagrees with the relatively thin oceanic crust (5 km) in the northern part of the study area, suggested by refraction data. A similar contradiction exists in the northeastern Gulf of Mexico, where the SDR complex is interpreted by many authors (Imbert and Philippe, 2005; Eddy et al., 2014; Liu et al., 2019), but the oceanic crust is known to be thinner than normal (Christeson et al., 2014), suggesting a slow-spreading regime usually related to a deficit of magmatic material. This is consistent with the slow to ultra-slow spreading rates determined by Filina et al. (2020b). However, Planke et al. (2000) show that the periods of significant magmatic addition may alternate with episodes of very limited volcanism in passive continental margins. In order to better comprehend the tectonic history of the Gulf of Mexico, the SDRs, igneous intrusions, the overall extent and the individual compartments of the pre-salt basin and the distinct crustal zones must be carefully documented along the Yucatan margin to be later compared with the corresponding features in the northeastern part of the basin as these represent the matching structures at the conjugate margins.

4. Conclusions

The integrated analysis of seismic data with gravity and magnetic fields was conducted for the western margin of the Yucatan peninsula. The following conclusions were drawn based on this joint analysis:

(1) Two distinct crustal zones were identified in the continental domain. The first one comprises stretched and intruded crust adjacent to OCB with a total thickness of ~10 km. Our analysis suggests the conditions close to the exhumation of the lower crust under the Yucatan salt basin. We conclude that the removal of the upper continental crust occurred during the final (post-salt) phase of continental rifting and led to local subsidence that explains an extensive Jurassic salt flow observed by other authors. The crust of the second zone under the carbonate platform appears to be mostly unstretched with a crustal thickness exceeding 30 km. The boundary between them is roughly coincident with the SDRs in the north and with the Campeche magnetic anomaly in the south.

(2) The pre-salt basin, consisting of several compartments, extends along the entire study area; it narrows to the north and eventually pinches out at the northernmost tip of the Yucatan peninsula. The width of individual compartments is up to 100 km and the thickness of the pre-salt section is up to 5 km.

(3) The SDR province is adjacent to the pre-salt basin in the northern part of the study area; it is up to 400 km long and up to 50 km wide. Higher magnetic susceptibility of the SDR complex is required to fit the observed magnetic signal. Our analysis does not support any SDRs under the Campeche salt basin in the south.

(4) Several highly magnetic intrusions in the lower continental crust are required to fit the observed magnetic signature. This is similar to the observations from the northern Gulf of Mexico.

The integrated approach in data analysis led to more confident results as the derived subsurface structures and the outlined tectonic regions honor multiple geophysical datasets. The results of this study are important for tectonic reconstruction of the Gulf of Mexico, as the presalt basins, SDR province, and individual crustal zones should be aligned on conjugate margins.

Declaration of competing interest – The authors declare that they have no known competing financial interests or personal relationships that could have appeared to influence the work reported in this paper.

Acknowledgments – The authors are extremely grateful to Jane Whaley, the editor of GEO ExPro, for help with obtaining permissions to reproduce published images from TGS and ION. Many thanks go to Carlos Williams-Rojas for providing the original images of seismic cross-sections. The authors also express their appreciation to Pedro Jose Carmona-Alegria, the editor of Ingeniería Petrolera, for providing the seismic image from Miranda-Peralta et al. (2014). We acknowledge the academic license from Geosoft that was used for modeling and spatial analysis.

Credit roles – Irina Filina: conceptualization, supervision, modeling, validation, writing—original draft, writing—review and editing; Lucas Hartford: modeling, writing—original draft.

References

Beutel, E., Filina, I., 2020. New Observations Suggest the Need for Revised Tectonic 1612 Reconstructions of the Gulf of Mexico. AAPG2020.

Buffler, R.X., Shipboard Scientific Party, 1984. Initial Report of the Deep Sea Drilling Project, ume 77. U.S. Government Printing Office, Washington, D.C., pp. 279–336. https://doi.org/10.2973/dsdp.proc.77.105.1984

Carlson, R.L., Herrick, C.N., 1990. Densities and porosities in the oceanic crust and their variations with depth and age. J. Geophys. Res. 95 (B6), 9153–9170.

Christensen, N., Mooney, W., 1995. Seismic velocity structure and composition of the continental crust: a global view. Journal of Geophysical Research Atmospheres 100, 9761–9788.

Christeson, G.L., Goff, J.A., Reece, R.S., 2019. Synthesis of oceanic crustal structure from two-dimensional seismic profiles. Rev. Geophys. 57, 504–529. https://doi.org/10.1029/2019RG000641

Christeson, G.L., Van Avendonk, H.J.A., Norton, I.O., Snedden, J.W., Eddy, D.R., Karner, G.G., Johnson, C.A., 2014. Deep crustal structure in the eastern Gulf of Mexico. J. Geophys. Res.: Solid Earth 119, 6782–6801.

Curry, M., Peel, F.J., Hudec, M.R., Norton, I., 2018. Extensional models for the development of passive-margin salt basins, with application to the Gulf of Mexico. Basin Res. 30, 1180–1199. https://doi.org/10.1111/bre.12299.

Davison, I., O'Beirne, E., Faull, T., Steel, I., 2015. Vast potential: Mexico's offshore ronda uno. GEO ExPro 12 (2), 68–71.

Dribus, J.R., Jackson, M., Kapoor, K., 2008. The prize beneath the salt. Oilfield Rev. 20, 4–17.

Eagles, G., Pérez-Díaz, L., Scarselli, N., 2015. Getting over continent ocean boundaries. Earth Sci. Rev. 151, 244–265. https://doi.org/10.1016/j.earscirev.2015.10.009.

Eddy, D., Van Avendonk, H., Christeson, G., Norton, I., Karner, G., Johnson, C., Snedden, J., 2014. Deep crustal structure of the northeastern Gulf of Mexico: implications for rift evolution and seafloor spreading. Journal of Geophysical Research Solid Earth 119 (9), 6802–6822. https://doi.org/10.1002/2014JB011311.

Eddy, D., Van Avendonk, H., Christeson, G., Norton, I., 2018. Structure and origin of the rifted margin of the northern Gulf of Mexico. Geosphere 14 (4), 1804–1817.

Ewing, J., Antoine, J., Ewing, M., 1960. Geophysical measurements in the western caribbean sea and in the gulf of Mexico. J. Geophys. Res. 65 (12), 4087–4126.

Filina, I., Delebo, N., Mohapatra, G., Coble, C., Harris, G., Layman, J., Strickler, M., Blangy, J.P., 2015. Integration of seismic and gravity data—a case study from the western Gulf of Mexico. Interpretation 3 (4), SAC99–SAC106.

Filina, I., Biegert, E., Sander, L., Tschirhart, V., Bundalo, N., Schiek-Stewart, C., 2019. Integrated imaging: a powerful but undervalued tool. Lead. Edge 38, 720–724. https://doi.org/10.1190/tle38090720.1. September 2019.

Filina, I., 2019. Crustal architecture of the northwestern and central Gulf of Mexico from integrated geophysical analysis. Interpretation 7 (4), 1–12. https://doi.org/10.1190/INT-2018-0258.1.

Filina, I., Austin, J.A., Doré, A.G., Johnson, E.A., Lundin, E., Minguez, D.A., Norton, I.O., Snedden, J., Stern, R.J., 2020a. December. The tectonic history of the gulf of Mexico—A comprehensive review to Chart new directions. In: AGU Fall Meeting 2020. AGU.

Filina, I., Liu, M., Beutel, E., 2020b. Evidence of ridge propagation in the eastern Gulf of Mexico from integrated analysis of potential fields and seismic data. Tectonophysics 775, 228307.

Galloway, W., 2009. Gulf of Mexico, 2009 GEO ExPro 6 (3), 22–26. n. 3.

Hilterman, F., 1998. Rock property framework for comprehending deep-water seismic response. In: 14th Annual Gulf Coast Technical Meeting. SEG.

Horn, B., Hartwig, A., Faw, J., Novianti, I., Goswami, A., McGrail, A., 2017. Evaluation of offshore Campeche salt basin with progressive data resolution. Geo Expro 14 (1), 64–69.

Hudec, M.R., Norton, I.O., Jackson, M.P.A., Peel, F.J., 2013. Jurassic evolution of the Gulf of Mexico salt basin. AAPG (Am. Assoc. Pet. Geol.) Bull. 97 (10), 1683–1710.

Hudec, M.R., Norton, I.O., 2019. Upper jurassic structure and evolution of the yucatan and Campeche subbasins. southern Gulf of Mexico: AAPG (Am. Assoc. Pet. Geol.) Bull. 103 (5), 1133–1151. May 2019.

Hunt, C.P., Moskowitz, B.M., Banerjee, S.K., 1995. Magnetic Properties of Rocks and Minerals, Classification of Rocks and Their Abundances on the Earth, pp. 189–204 (3-l).

Ibrahim, A.K., Carye, J., Latham, G., Buffler, R.T., 1981. Crustal structure in gulf of Mexico from OBS refraction and multichannel reflection data. AAPG (Am. Assoc. Pet. Geol.) Bull. 65 (7), 1207–1229.

Imbert, P., Phillippe, Y., 2005. The mesozoic opening of the gulf of Mexico: Part 1, evidence for oceanic accretion during and after salt deposition. In: Post, P.J., Rosen, N.C., Olson, D.L., Palmes, S.L., Lyons, K.T., Newton, G.B. (Eds.), Transactions of the 25th Annual GCSSEPM Research Conference: Petroleum Systems of Divergent Continental Margins, pp. 1151–1189. https://doi.org/10.5724/gcs.05.25.1119.

Li, C.-F., Lu, Y., Wang, J., 2017. A global reference model of Curie-point depths based on EMAG2. Sci. Rep. 7, 45129. https://doi.org/10.1038/srep45129.

Liu, M., Filina, I., Mann, P., 2019. Crustal structure of Mesozoic rifting in the northeastern Gulf of Mexico from the integration of seismic and potential fields data. Interpretation 7 (4). https://doi.org/10.1190/int-2018-0259.1.

Lundin, E.R., Doré, A.G., 2017. The Gulf of Mexico and Canada Basin: genetic siblings on either side of North America. GSA Today (Geol. Soc. Am.) 27 (1), 4–11.

Meyer, B., Saltus, R., Chulliat, A., 2017. EMAG2: Earth Magnetic Anomaly Grid (2-Arc-Minute Resolution). National Centers for Environmental Information, NOAA. https://doi.org/10.7289/V5H70CVX version 3.

Miranda-Peralta, L.R., Cardenas-Alvarado, A., Maldonado-Villalon, R., Reyes-Tovar, E., Ruiz-Morales, J., Williams-Rojas, C., 2014. Play hipotetico pre-sal en aguas profundas del Golfo de Mexico. Ingenierıa Petrolera 54, 256–266.

Nguyen, L.C., Mann, P., 2016. Gravity and magnetic constraints on the Jurassic opening of the oceanic Gulf of Mexico and the location and tectonic history of the Western Main transform fault along the eastern continental margin of Mexico. Interpretation 4 (1), SC23–SC33.

O'Reilly, C.O., Keay, J., Birch-Hawkins, A., Bate, D., Halliday, J., 2017. Regional play types in the Mexican offshore. GEO ExPro 14 (4), 36–45.

Pindell, J.L., Miranda, C.E., Cerón, A., Hernandez, L., 2016. Aeromagnetic map constrains jurassic-early cretaceous synrift, break up, and rotational seafloor spreading history in the gulf of Mexico. In: Lowery, C.M., Snedden, J.W., Rosen, N.C. (Eds.), Mesozoic of the Gulf Rim and beyond: New

Progress in Science and Exploration of the Gulf of Mexico Basin, vol. 35. SEPM Society for Sedimentary Geology. https://doi.org/10.5724/gcs.15.35.0123.

Planke, S., Symonds, P.A., Alvestad, E., Skogseid, J., 2000. Seismic volcanostratigraphy of large-volume basaltic extrusive complexes on rifted margins. J. Geophys. Res.: Solid Earth 105 (B8), 19335–19351.

Salem, A., Williams, S., Fairhead, D., Smith, R., Ravat, D., 2008. Interpretation of magnetic data using tilt-angle derivatives. Geophysics 73 (1), L1–L10. https://doi.org/10.1190/1.2799992.

Sandwell, D.T., Muller, R.D., Smith, W., Garcia, E., Francis, R., 2014. New global marine gravity model from CryoSat-2 and Jason-1 reveals buried tectonic structure. Science 346, 65–67.

Saunders, A., Geiger, L., Rodrigues, K., Hargreaves, P., 2016. The delineation of pre-salt license blocks in the deep offshore Campeche-Yucatan basin. In: AAPG Annual Convention and Exhibition, Calgary, Alberta, Canada, Search and Discovery. Article #10867.

Seelke, C.R., Ratner, M., Villarreal, M.A., Brown, P., 2013. Mexico's Oil and Gas Sector: Background, Reform Efforts, and Implications for the United States. Congressional Research Service.

Steier, A., Mann, P., 2019. Late Mesozoic gravity sliding and Oxfordian hydrocarbon reservoir potential of the northern Yucatan margin. Mar. Petrol. Geol. 103, 681–701.

Telford, W.M., Geldart, L.P., Sheriff, R.E., 1990. Applied Geophysics. Cambridge University Press.

Van Avendonk, H.J., Christeson, G.L., Norton, I.O., Eddy, D.R., 2015. Continental rifting and sediment infill in the northwestern Gulf of Mexico. Geology 43 (7), 631–634.

Weatherall, P., Marks, K.M., Jakobsson, M., Schmitt, T., Tani, S., Arndt, J.E., Rovere, M., Chayes, D., Ferrini, V., Wigley, R., 2015. A new digital bathymetric model of the world's oceans. Earth and Space Science 2 (8), 331–345.

Whaley, J., 2006. Huge Potential Still Waiting in the Gulf of Mexico, vol. 3. GeoExPro, pp. 14–24.

Williams-Rojas, C.T., Reyes-Tovar, E., Miranda-Peralta, L., Reyna-Martinez, G., Cardenas-Alvarado, A., Maldonado-Villalon, R., Muñoz-Bocanegra, V., Lora-delaFuente, C., 2012. Hydrocarbon potential of the deepwater portion of "Salina del Istmo" province, southeastern Gulf of Mexico, Mexico. Gulf Coast Association of Geological Societies Transactions 61, 681–684.